**TECHNICAL REPORT STANDARD PAGE**

| 1. Report No. | 2. Government Accession No. | 3. Recipient's Catalog No. |
|---|---|---|
| **FHWA/LA.08/424** | | |

| 4. Title and Subtitle | 5. Report Date |
|---|---|
| **Use of Reinforced Soil Foundation (RSF) to Support Shallow Foundation** | **May 2008** |
| | 6. Performing Organization Code<br>**LTRC Number: 04-2GT**<br>**State Project Number: 736-99-1242** |
| 7. Author(s)<br>**Murad Y. Abu-Farsakh, Ph.D., P.E., and Qiming Chen, Ph.D.** | 8. Performing Organization Report No.<br>**424** |
| 9. Performing Organization Name and Address<br>**Louisiana Transportation Research Center**<br>**4101 Gourrier Avenue**<br>**Baton Rouge, LA 70808** | 10. Work Unit No.<br><br>11. Contract or Grant No.<br>**04-2GT** |
| 12. Sponsoring Agency Name and Address<br>**Louisiana Transportation Research Center**<br>**4101 Gourrier Avenue**<br>**Baton Rouge, LA 70808** | 13. Type of Report and Period Covered<br>**Summary Report**<br>**March 2004 – December 2007**<br>14. Sponsoring Agency Code |

15. Supplementary Notes
**Conducted in Cooperation with the U.S. Department of Transportation, Federal Highway Administration**

16. Abstract

This research study investigates the potential benefits of using reinforced soil foundations to improve the bearing capacity and reduce the settlement of shallow foundations on soils. To implement this objective, a total of 117 tests, including 38 laboratory model tests on silty clay embankment soil, 51 laboratory model tests on sand, 22 laboratory model tests on Kentucky crushed limestone, and 6 large-scale field tests on silty clay embankment soil were performed at the Louisiana Transportation Research Center to study the behavior of reinforced soil foundations. The influences of the different variables and parameters contributing to the improved performance of reinforced soil foundation were examined in these tests. In addition, an instrumentation program with pressure cells and strain gauges was designed to investigate the stress distribution in soil mass with and without reinforcement and the strain distribution along the reinforcement. The test results showed that the inclusion of reinforcement can significantly improve the soil's bearing capacity and reduce the footing settlement. The geogrids with higher tensile modulus performed better than geogrids with lower tensile modulus. The strain developed along the reinforcement is directly related to the settlement, and, therefore, higher tension would be developed for geogrid with higher modulus under the same footing settlement. The test results also showed that the inclusion of reinforcement will redistribute the applied load to a wider area, thus minimizing stress concentration and achieving a more uniform stress distribution. The redistribution of stresses below the reinforced zone will result in reducing the consolidation settlement of the underlying weak, clayey, soil which is directly related to the induced stress. Insignificant strain measured in the geogrid beyond its effective length of 4.0 ~ 6.0B indicated that the geogrid beyond this length provides a negligible extra reinforcement effect.

| 17. Key Words | 18. Distribution Statement |
|---|---|
| **Reinforced soil foundation, Geosynthetics, Laboratory model test, Large-scale test, Soil, Bearing capacity ratio, Settlement reduction factor, Instrumentation, Vertical stress, Strain.** | **Unrestricted. This document is available through the National Technical Information Service, Springfield, VA 21161.** |

| 19. Security Classif. (of this report) | 20. Security Classif. (of this page) | 21. No. of Pages | 22. Price |
|---|---|---|---|
| **Unclassified** | **Unclassified** | **55** | |

# Use of Reinforced Soil Foundation (RSF) to Support Shallow Foundation

**Summary Report**

by
Murad Y. Abu-Farsakh, Ph.D., P.E.
Qiming Chen, Ph.D.

Louisiana Transportation Research Center
4101 Gourrier Avenue
Baton Rouge, LA 70808

LTRC Project No. 04-2GT
State Project No. 736-99-1242

conducted for

Louisiana Department of Transportation and Development
Louisiana Transportation Research Center



November 2008

# IMPLEMENTATION STATEMENT

An experimental testing program including four series of small-scale and large-scale model footing tests was conducted to investigate the benefits of reinforcing soil foundation (RSF) and to study the influence of different design parameters on the improved performance of reinforced soil foundation. The test results clearly demonstrated that the use of reinforcements can significantly increase the bearing capacity of soil foundations and reduce footing settlement.

Analyses of the test results enabled us to derive/modify analytical design procedures for reinforced soil foundations that include the effects of different design variables needed for implementation. The authors recommended a step-by-step procedure for designing RSF. The RSF can be implemented in many geotechnical engineering applications, such as foundations for earth-retaining structures, working platforms for embankment construction, working platforms over soft subgrades for pavement applications, reinforced-soil pile-support caps, reinforced-soil abutments, and foundations for residential and commercial buildings.

One potential implementation is the use of RSF in the design of approach slab for highway engineering applications to minimize the resulting differential settlements. Since the state of Louisiana is renowned for its weak, natural soil formations, the common result of excessive differential settlement of the concrete approach slab currently creates one of the major highway maintenance problems. To solve this problem, the Louisiana Quality Initiative (LQI) study recommended changing the design of approach slabs by increasing its rigidity. As a result, the slab and traffic loads will be carried by the two ends of the slab rather than distributed over the length of the slab. Accordingly, a strip footing will be needed at the far end of the approach slab away from the bridge. To increase the soil's bearing capacity and minimize settlement due to concentration load, the soil underneath the strip footing will be reinforced. Implementation of this research project can lead to a better design of approach slabs with improved performance and significant savings due to expected reduced maintenance and better rideability.

# TABLE OF CONTENTS

# LIST OF TABLES

# LIST OF FIGURES

# INTRODUCTION

The presence of a weak soil (clay) supporting structural foundations (footings) results in low load bearing capacity and excessive settlements, which can cause structural damage, reduction in durability, and/or deterioration in performance level. Conventional treatment methods were to replace part of the weak cohesive soil with an adequately thick layer of stronger granular fill, increase the dimensions of the footing, or a combination of both methods. However, an alternative and more economical solution is the use of geosynthetics to reinforce soils, which can be done by either reinforcing cohesive soil directly or replacing the poor soils with stronger granular fill in combination with the inclusion of geosynthetics. The resulting composite zone (reinforced soil mass) will improve the load carrying capacity of the footing and provide better pressure distribution on top of the underlying weak soils, hence reducing the associated settlements.

One potential application is the use of reinforced soil foundations (RSF) in the design of approach slabs for highway engineering applications to minimize the resulting differential settlements immediately under the approach slab bearing location. Excessive differential settlement of the concrete approach slab currently causes a significant bridge “bump” problem, resulting in uncomfortable rides and frequent repairs. Methods to prevent the bump from developing have involved the improvement of the natural soil under the embankment, the use of selected embankments, and the use of piles with decreasing lengths supporting the approach slab. One proposed solution is to use a rigid approach slab and transfer the traffic loads to the two ends of the slab. Accordingly, a shallow foundation is needed at the end of the approach slab far from the bridge to carry that part of load. To achieve better bearing capacity and/or to prevent excessive settlement, the soil underneath the footing needs to be reinforced; the designer will still need to consider roadway embankment settlement in the design.

The benefits of the inclusion of reinforcements within soil mass to increase the bearing capacity and reduce the settlement of soil foundation have been widely recognized. Many hypotheses have been postulated about the failure mode of RSF. However, the failure mechanism of reinforcement is still not fully understood in RSF as compared to other reinforced soil applications. Therefore, it is important to investigate the reinforcement mechanism of reinforcing soils for foundation applications.

# OBJECTIVE

The main objective of this research study is to investigate the potential benefits of using reinforced soil foundations to improve the bearing capacity and to reduce the settlement of shallow foundations on soils. These include: (1) examining the influences of different variables and parameters contributing to the improved performance of RSF, (2) investigating the stress distribution in soil mass with and without reinforcement and the strain distribution along reinforcements, (3) understanding the failure mechanism of reinforced soil, (4) developing regression models to estimate the bearing capacity of RSFs, and (5) conducting stability analysis of reinforced soil foundations and developing a step-by-step procedure for the design of reinforced soil foundations.

# SCOPE

This research project included conducting small-scale laboratory model footing tests on silty clay soil, sandy soil, and crushed limestone, in addition to large-scale field tests on silty clay soil. The model footings used in the laboratory tests were 1 in. thick steel plates with dimensions of 6 in. × 6 in. and 6 in. × 10 in. The model footing used in the field tests was 8 in. thick, reinforced precast concrete block with dimensions of 1.5 ft. × 1.5 ft. The experimental study also includes investigating the stress distribution in the soil mass with and without reinforcement and the strain distribution along the reinforcement. Based on the results of this study, existing analytical solutions were examined, and new methods based on limit equilibrium analysis were proposed to calculate the bearing capacity of RSF for different soil types.

# RESEARCH APPROACH

The testing program included conducting both small-scale and large-scale model footing tests on three soil types (sand, silty clay, and crushed limestone) to investigate the influence of different parameters involved in the design of RSF. The experimental study also includes the investigation of the stress distribution in the soil mass with/without reinforcement and the strain distribution along the reinforcement. A brief description of the testing program will be presented here. Full details of the testing program can be found in the final report (FHWA/LA08/423).

## Properties of Tested Materials

### Soils

Three different soil types were used in this study, sand, silty clay, and Kentucky crushed limestone. The properties of these soils are summarized in tables 1, 2 and 3, respectively.

**Table 1**
**Properties of sandy soil**

| Property | Value |
|---|---|
| Effective particle size ($D_{10}$) | 0.0089 in. |
| Mean particle size ($D_{50}$) | 0.0177 in. |
| Uniformity coefficient ($C_u$) | 2.07 |
| Coefficient of curvature ($C_c$) | 1.25 |
| Maximum dry density[#] | 101 lb/ft$^3$ |
| Optimum moisture content[#] | 4.8% |
| USCS | SP |
| AASHTO | A-1-b |
| Friction angle* | 44$^o$ to 48$^o$ |

**Table 2**
**Properties of silty clay/embankment soil**

| Property | Value |
|---|---|
| Liquid limit | 31 |
| Plastic index | 15 |
| Silt content | 72% |
| clay content | 19% |
| Maximum dry density[#] | 104 lb/ft$^3$ |
| Optimum moisture content[#] | 18.75% |
| USCS | CL |
| AASHTO | A-6 |
| Cohesion intercept* | 0.73 psi to 3.57 psi |
| Friction angle* | 25.96$^o$ to 24.13$^o$ |

**Table 3**
**Properties of Kentucky crushed limestone**

| Property | Value |
|---|---|
| Effective particle size ($D_{10}$) | 0.0183 in. |
| Mean particle size ($D_{50}$) | 0.2189 in. |
| Uniformity coefficient ($C_u$) | 20.26 |
| Coefficient of curvature ($C_c$) | 1.37 |
| Maximum dry density[#] | 142 lb/ft$^3$ |
| Optimum moisture content[#] | 7.5% |
| USCS | GW |
| AASHTO | A-1-a |
| Friction angle* | 53$^o$ |

[#] Standard Proctor test
* Large-scale direct shear tests on sand at maximum dry density

### Reinforcement

Nine types of geosynthetics (eight geogrid types and one geotextile type), one type of steel wire mesh, and one type of steel bar mesh were used in the present study. The physical and mechanical properties of these reinforcements as provided by the manufacturers are summarized in table 4.

**Table 4**
**Properties of reinforcements**

| Reinforcement | Polymer Type | T[a], lb/ft | | J[b], lb/ft | | Aperture Size, in |
|---|---|---|---|---|---|---|
| | | MD[c] | CD[d] | MD[c] | CD[d] | |
| Mirafi BasXgrid11 geogrid | Polyester | 500 | 500 | 25000 | 25000 | 1.0×1.0 |
| Tensar BX6100 geogrid | Polypropylene | 250 | 350 | 12500 | 17500 | 1.3×1.3 |
| Tensar BX6200 geogrid | Polypropylene | 375 | 510 | 18750 | 25500 | 1.3×1.3 |
| Tensar BX1100 geogrid | Polypropylene | 280 | 450 | 14000 | 22500 | 1.0×1.3 |
| Tensar BX1200 geogrid | Polypropylene | 410 | 620 | 20500 | 31000 | 1.0×1.3 |
| Tensar BX1500 geogrid | Polypropylene | 580 | 690 | 29000 | 34500 | 1.0×1.2 |
| Tenax MS330 Geogrid | Polypropylene | 418 | 616 | 20900 | 30800 | 1.65×1.96[*] |
| Mirafi Miragrid 8XT geogrid | Polyester | 1095 | 5480 | 54750 | 274000 | 0.875× 1.0 |
| Mirafi HP570 geotextile | Polypropylene | 960 | 1320 | 48000 | 66000 | ≈ 0 |
| Steel Wire Mesh | Stainless Steel | 16170 | 30630 | 808500 | 1531500 | 1.0×2.0 |
| Steel Bar Mesh | Steel | 66470 | 66470 | 3323500 | 3323500 | 3.0×3.0 |

[a]Tensile Strength (at 2% strain), [b] Tensile Modulus (at 2% strain),
[c]Machine Direction, [d]Cross Machine Direction, [*]Single Layer Dimension

## Testing Program

### Small-Scale Laboratory Tests

The laboratory model footing tests were conducted inside a steel box with dimensions of 5 ft. (length) × 3 ft. (width) × 3 ft. (height). The model footings used in the tests were 1 in. thick

steel plates with dimensions of 6 in. × 6 in. and 6 in. × 10 in. The soil was compacted inside the box using an 8 in. × 8 in. plate adapted to a vibratory jack hammer. The nuclear density gauge and the geogauge stiffness device were used to control the construction of each soil lift. The footings were loaded with a hydraulic jack against a reaction steel frame. The testing procedure was performed according to the ASTM D 1196-93, where the load increments were applied and maintained until the rate of settlement was less than 0.001 in/min for three consecutive minutes. The load and the corresponding footing settlement for unreinforced and reinforced soils were measured using a ring load cell and two dial gauges, respectively.

The test sections were instrumented with earth pressure cells (Geokon Model 4800 VW) to measure the vertical stress distribution in the soil and electrical resistance strain gauges (EP-08-250BG) to measure the distribution along the reinforcement. Figure 1 shows a complete test-up, loading and reaction system, and instrumentation system used in the laboratory model tests.

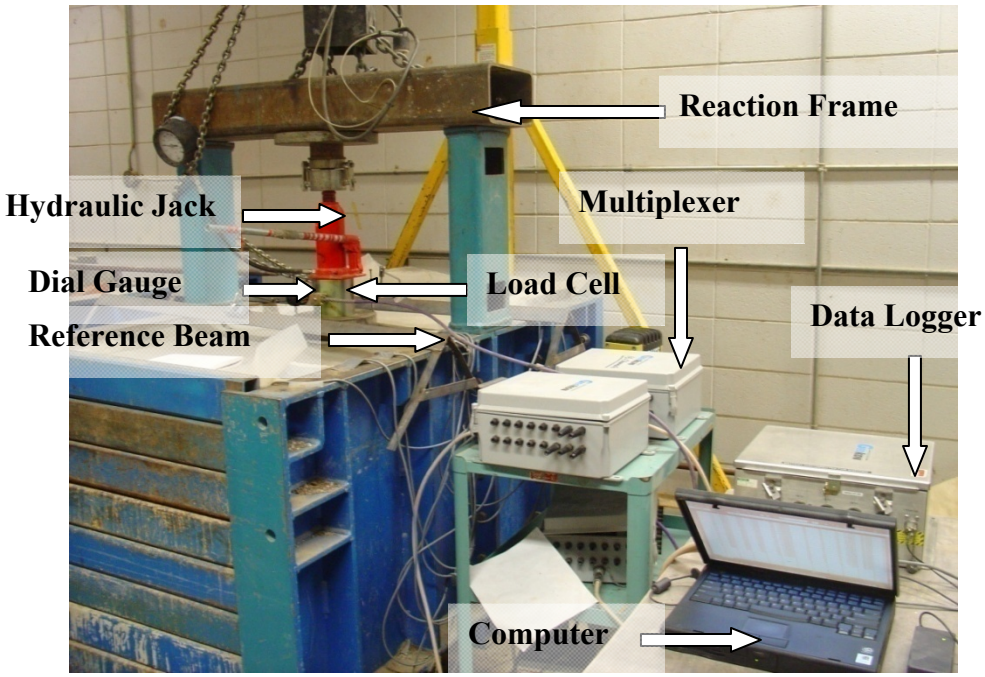


**Figure 1**
**Laboratory test set up and instrumentation system**

**Large-Scale Field Tests**

A total of six large-scale model footing tests were performed in an outdoor test pit constructed next to the LTRC building. The test pit has a dimension of 12 ft. (length) × 12 ft. (width) × 6 ft. (height). The soil was mixed with water using a tiller and compacted in lifts

using a MultiQuip plate compactor and a Wacker-Packer tamper. The nuclear density gauge and the geogauge stiffness device were used to measure the density and stiffness modulus for construction control of each lift. The load was applied on the footing by a hydraulic jack supported against a steel beam-steel piles reaction frame. A load cell was used to measure the applied load. The settlement was measured using dial gauges mounted on reference beams. The model footing used in the field tests was 8 in. thick, reinforced concrete block with dimensions of 1.5 ft. × 1.5 ft. The soil selected for large-scale model tests was the silty clay soil. The large-scale tests were performed according to the ASTM D 1196-93. A complete field test set up and instrumentation system is shown in figure 2.

**Figure 2**
**Field test set up and instrumentation system**

## DISCUSSION OF RESULTS

In this study, two terms were used to evaluate the benefits of using RSF. The bearing capacity ratio (BCR), which is defined as the ratio of the bearing capacity of the RSF to that of the un-reinforced and the settlement reduction factor (SRF), which is defined as the ratio of the settlement of the RSF to that of the unreinforced. Two different types of load-settlement behavior were observed in the model footing tests. For the first type of load-settlement curve as show in figure 3a, the failure point is not well defined. The benefits of using RSF were then evaluated in terms of BCR at a specific settlement ($BCR_s$) and RSF at a specific surface pressure. Figure 3b depicts the second type of load-settlement curve which has a well defined failure point. For this type of load-settlement behavior, BCR at a specific settlement ($BCR_s$), BCR at the ultimate bearing capacity ($BCR_u$) and SRF at a specific surface pressure were used to evaluate the improved performance of RSF.

Figure 4 depicts a typical geosynthetic RSF with the meaning of geometric parameters used in the present study. The optimal values for reinforcement layout and the effect of types of reinforcement and soil are determined based on BCR and SRF. The discussion also includes stress distribution in soil with/without reinforcement and strain distribution along the reinforcement.

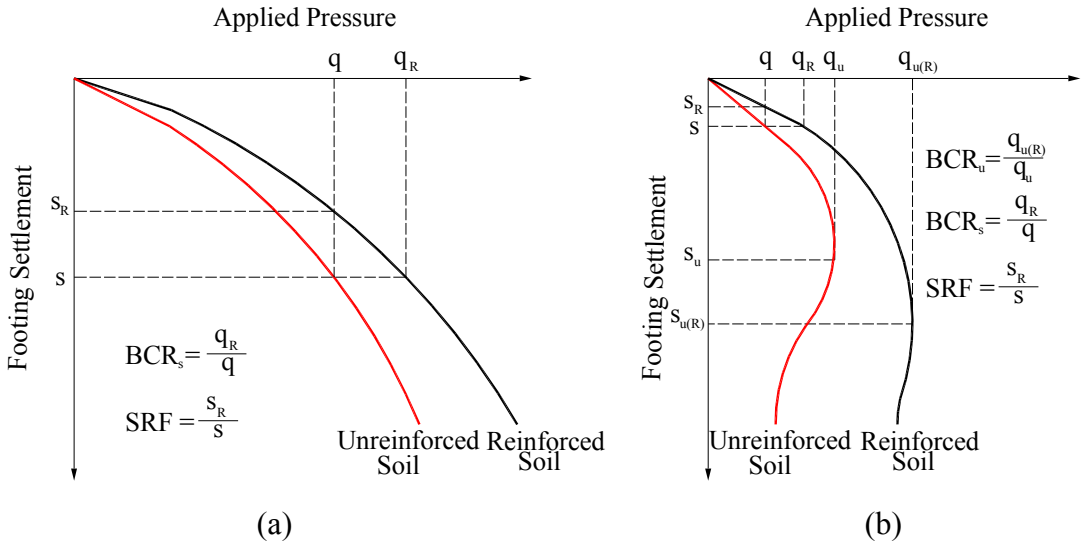


**Figure 3**
**Definitions of BCR and SRF**

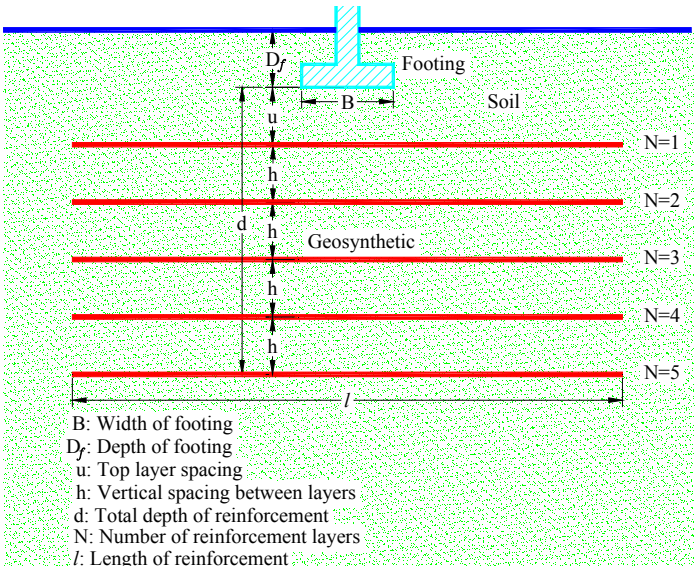


**Figure 4**
**Geosynthetic reinforced soil foundation**

### Effect of Reinforcement Top Spacing

The optimum location of the first reinforcement layer was investigated in the laboratory model footing tests on silty clay and sand soils reinforced using BasXgrid11 and Miragrid 8XT reinforcements. Figures 5a and 5b (for example) show that the BCRs at different settlement ratios increase with increasing the top layer spacing ratios (*u/B*) up to a maximum value of *u/B* = 0.33, after which it decreases. The top layer spacing ratio (*u/B*) is defined as the ratio of top layer spacing (*u*) to footing width (B). The optimum location of the top layer is then estimated to be about 0.33B.

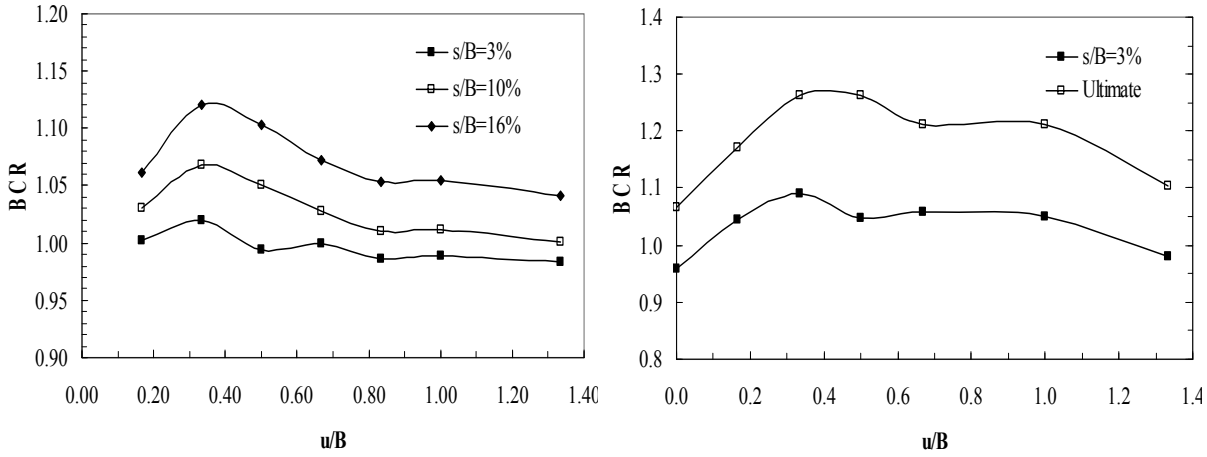


(a) Silty clay soil (b) Sand soil

**Figure 5**
**BCR versus *u/B* for one layer of reinforcement of BasXgrid11**

## Effect of Number of Reinforcement Layers

A series of laboratory model footing tests were conducted on the three soils reinforced with multiple layers of different types of geosynthetics, placed at a spacing of 0.33B, to investigate the influence depth of reinforcement (d). The effect of number of reinforcement layers was also investigated in the large-scale tests using multi-layers of BX6200 geogrid with a top layer spacing of 0.33B. Figures 6a and 6b present examples of the variations of BCRs obtained at different settlement ratios with the numbers of reinforcement layers (N), and hence the reinforcement depth ratios (d/B), for reinforced silty clay and reinforced sand, respectively. The reinforcement depth ratio is defined as the ratio of the total depth of reinforcement (d) to footing width (B). As expected, the bearing capacity increased with increasing number of reinforcement layers. However, the significance of an additional reinforcement layer decreases with the increase in number of layers. This effect becomes negligible below the influence depth. The influence depth is the total depth of reinforcement below which the rate of increase in BCR is negligible with an additional reinforcement layer. It can be seen from these figures that the BCRs increase with N and d/B and appear to become almost constant between N=4 (d/B=1.33) and N=5 (d/B=1.67) for geogrid reinforced silty clay and between N=3 (d/B=1.0) and N=4 (d/B=1.33) for reinforced sand and geotextile reinforced silty clay. Accordingly, the authors estimated the influence depth to be 1.5B for geogrid reinforced clay and 1.25 B for reinforced sand and geotextile reinforced clay.

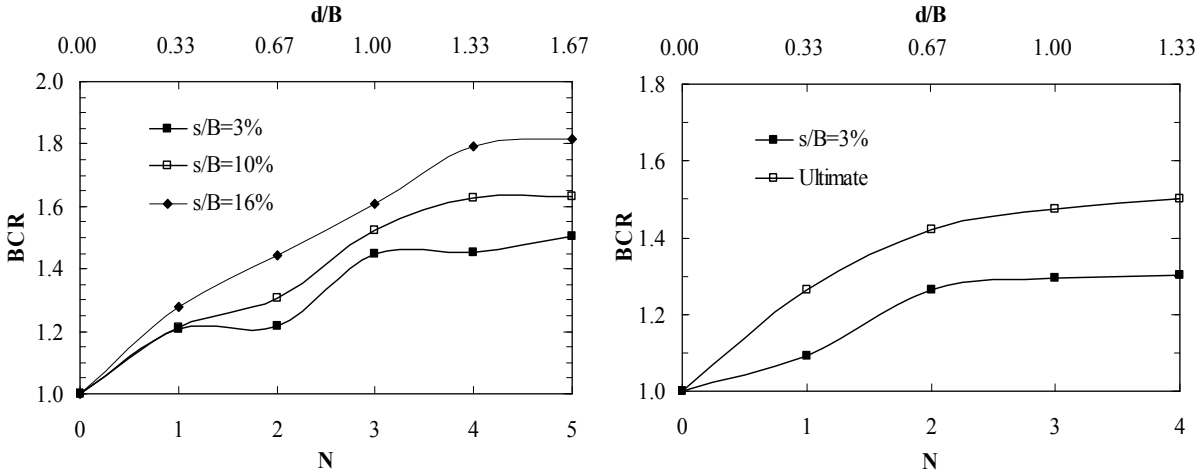


(a) BX6200 geogrid reinforced silty clay soil (b) BasXgrid11 geogrid reinforced sand soil

**Figure 6**
**BCR versus *N* and *d/B***

## Effect of Vertical Spacing of Reinforcement Layers

The effect of vertical spacing of reinforcement layers was investigated in the laboratory model tests using three layers of BX6200 geogrid for silty clay and three layers of

BasXgrid11 geogrid for sand with a top layer spacing of 2 in. (0.33B). The vertical spacing of reinforcement varied from 0.167B to 0.667B for silty clay and from 0.167B to 0.5B for sand. Figures 7a and 7b depict the variation in the BCR values obtained for different settlement ratios as a function of the vertical spacing ratio (*h/B*), which is defined as the ratio of the vertical spacing of reinforcement layers (*h*) to the footing width (*B*). It is obvious that the BCR values decrease with increasing vertical spacing of reinforcement layers with a maximum BCR value at *h* = 0.167B. The effect of vertical spacing on BCR is not independent from other parameters. In fact, it is a function of the top layer spacing (*u*), number of reinforcement layers (*N*), and reinforcement modulus. In design practice, engineers have to balance between using smaller spacing of lower geogrid modulus and using larger spacing of higher geogrid modulus.

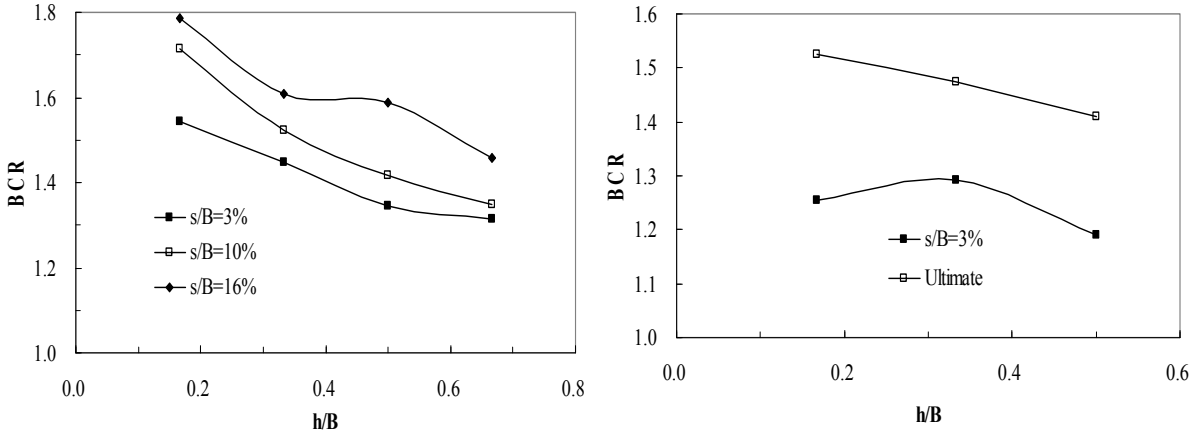


(a) Three layers of BX6200 geogrid in silty clay

(b) Three layers of BasXgrid11 geogrid in sand

**Figure 7**
**BCR versus *h/B* ratio**

**Effect of Tensile Modulus/Type of Reinforcement**

The effect of tensile modulus and type of reinforcement was investigated using both the laboratory and large-scale model footing tests on the three soil types. Different types of reinforcement with different tensile modulus were used in these tests as summarized in table 1. Figure 8a presents the BCRs obtained for silty clay soil reinforced with multiple layers of BasXgrid11, BX6100 geogrid, BX6200 geogrid, and HP570 geotextile, figure 8b presents the BCRs obtained for sand soil reinforced with multiple layers of BasXgrid11 geogrid, BX6100 geogrid, HP570 geotextile and HP570/BX6100 composite; and figure 8c presents the BCRs obtained for crushed limestone reinforced with multiple layers of BX1100 geogrid, BX1200 geogrid, BX1500 geogrid, BasXgrid 11, MS330 geogrid, Steel Wire Mesh (SWM), and Steel Bar Mesh (SWB). The figures demonstrate that the performance of

reinforced soil improves with increasing geogrid tensile modulus. However, the effect of the tensile modulus seems to be a function of settlement. The variations of BCRs with settlement ratios (s/B) for model footing tests on sand reinforced with multiple layers of different types of reinforcements are presented in figure 9. It can be seen that the BCR generally increases with the increase of settlement ratio (*s/B*). The settlement reduction factors (SRF) at different footing pressures (q) for the model footing tests on silty clay soil reinforced with multiple layers of BX6200 geogrid (for example) are presented in figure 10. It is obvious that the inclusion of reinforcement would reduce the immediate settlement significantly. With three or more layers of reinforcement, the settlement can even be reduced by 50 percent at a footing pressure of 58 psi. The higher tensile modulus geogrids provide the better reduction in immediate settlement than the lower tensile modulus geogrids.

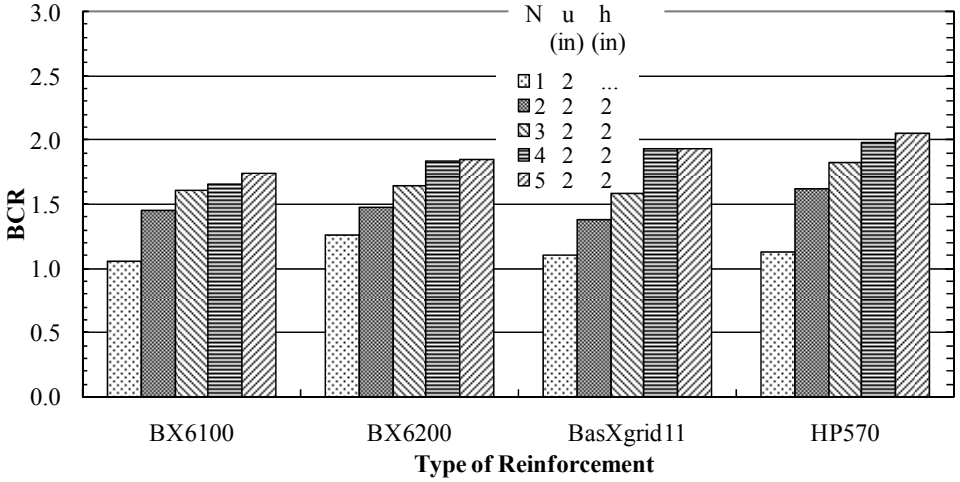


(a) Silty clay soil (s/B=24%)

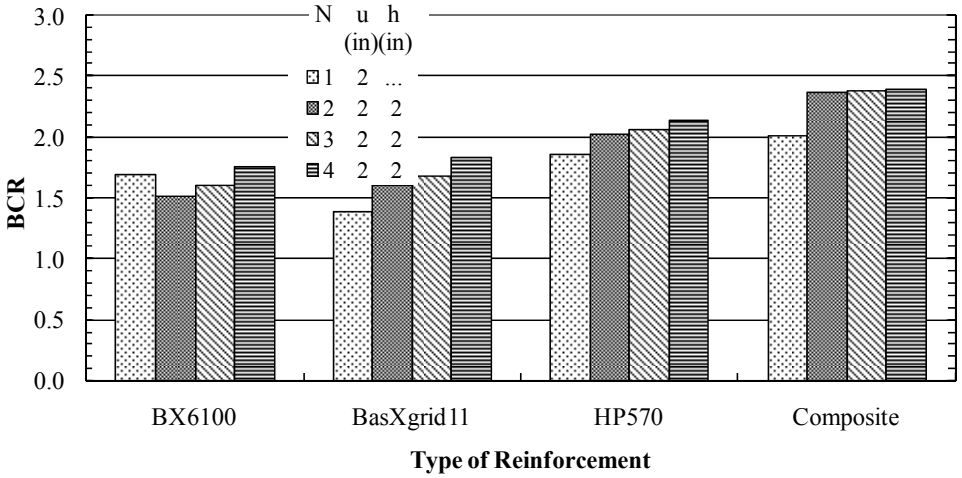


(b) Sand soil (s/B=12%)

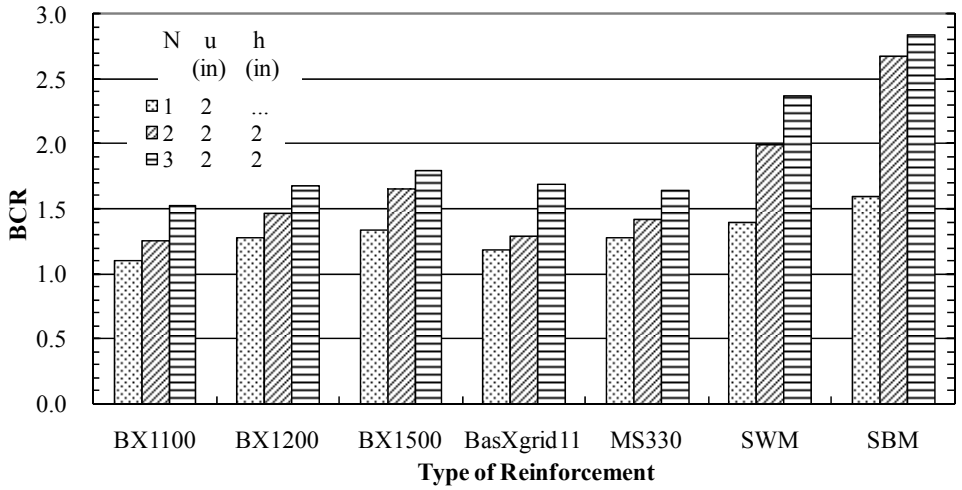


(c) Crushed limestone s/B = 10%

**Figure 8**
**BCR versus type of reinforcement**

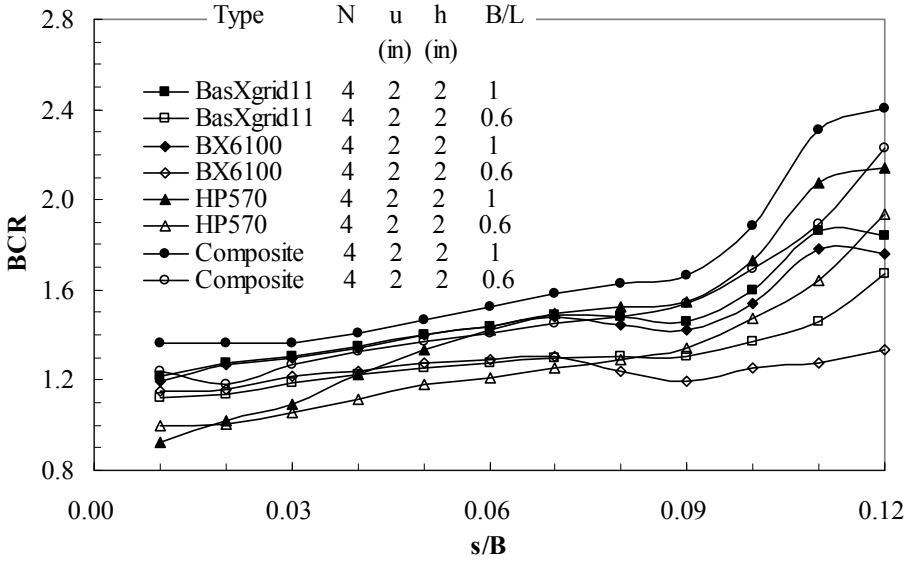


**Figure 9**
**BCR versus settlement ratio (s/B) ($D_f/B$ = 1.0)**

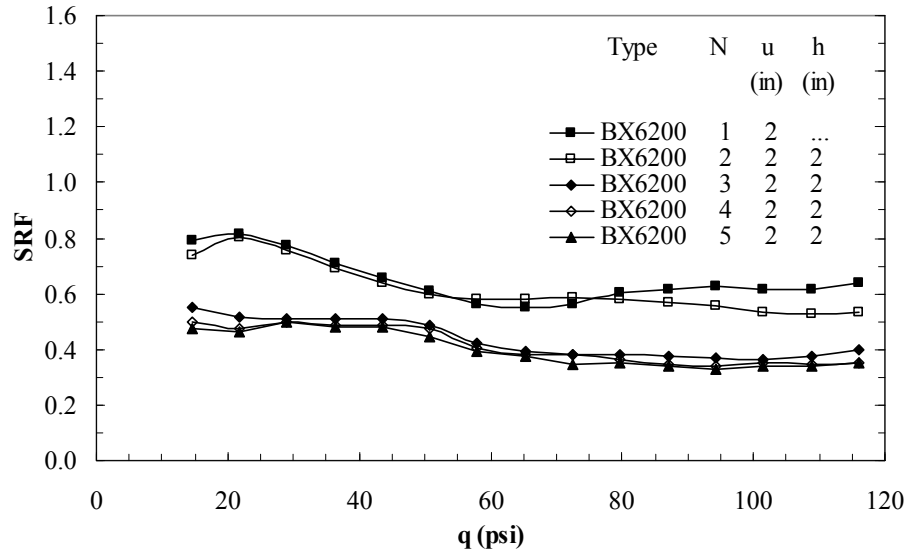


**Figure 10**
**SRF versus applied footing pressure (q)**

**Vertical Stress Distribution for Reinforced Soils**

Laboratory small-scale and field large-scale model tests were also used to evaluate the stress distribution in the silty clay and sand soils with and without reinforcement inclusion. Pressure cells were placed at specified locations/depths for this purpose. Examples of measured stress distributions along the center line of the footing at a depth of 1.67B below the footing are shown in figures 11a and 11b for laboratory model footing test and large-scale field model footing test of reinforced silty clay soil, respectively. It should be noted that the

stresses measured here by the pressure cells are the total vertical stresses induced by the applied load, not including the stresses induced by the weight of soil. As can be seen from these figures, the reinforcement resulted in redistribution of the vertical load to a wider area, thus reducing stress concentration and achieving improved stress distribution. This improved stress distribution below the influence depth is expected to decrease the total consolidation settlement of the footing, which is directly related to the induced stresses.

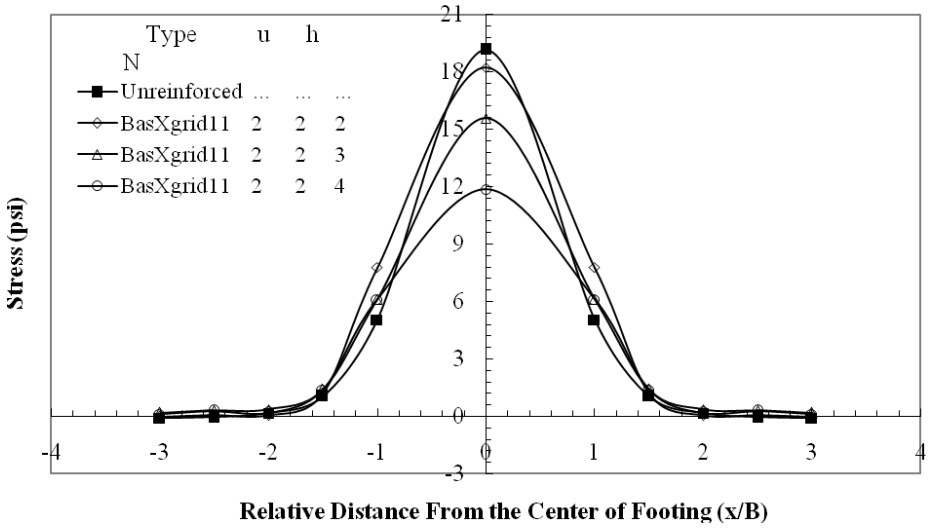


(a) Small-scale laboratory model footing tests

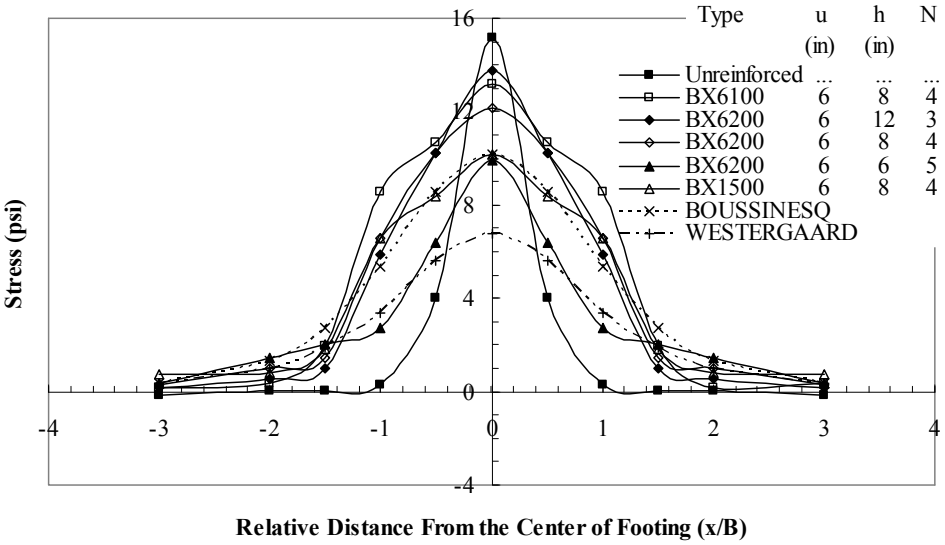


(b) Large-scale field model footing test

**Figure 11**
**Stress distributions along the center line of footing at a depth of 1.67B below the footing**

**Strain Distribution along Reinforcement**

The strain distribution along the reinforcement layers due to applied footing load was also investigated in this study. Some reinforcement layers during laboratory and field model footing tests were instrumented with strain gauges to measure the strain distribution along the these reinforcements. The variations of strains along the centerline of BX6100 geogrid measured at different settlement ratios(s/B) on reinforced silty clay are shown in figures 12a and 12b for small-scale and large-scale model footing tests, respectively. The measured tensile strain was maximum at the point beneath the center of the footing and becomes almost negligible at about 2.0 ~ 3.0B from the center of footing. This indicates that the geogrid beyond the effective length of $l_e$ = 4.0 ~ 6.0B results in insignificant mobilized tensile strength, and thus provides negligible effects on the improved performance of reinforced soil foundations.

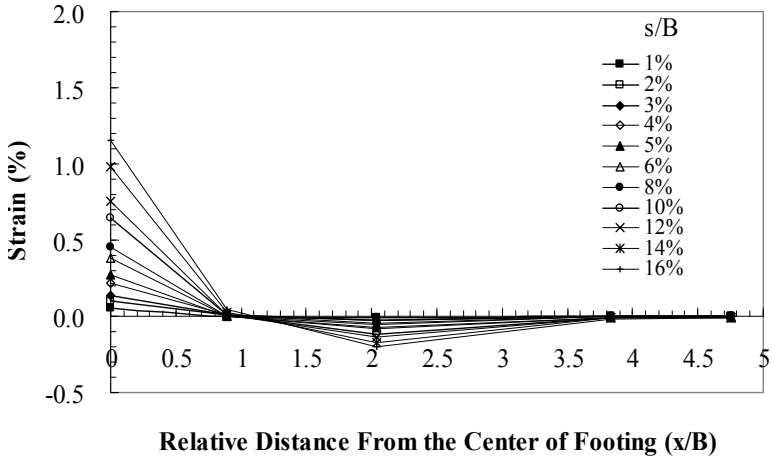


(a) Small-scale laboratory model footing tests

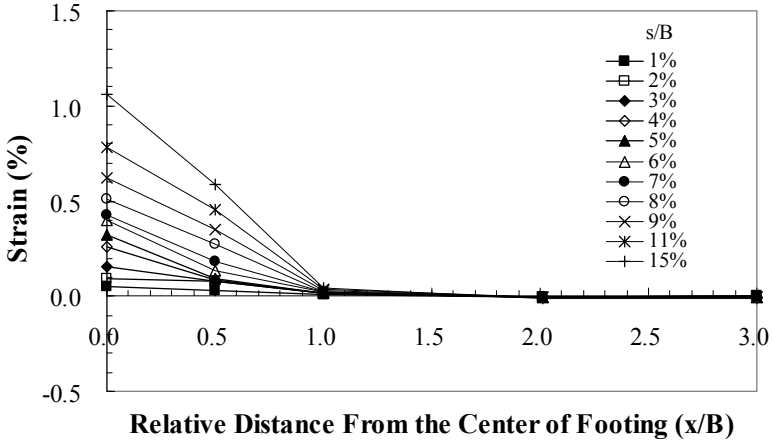


(b) Large-scale field model footing test

**Figure 12**
**Strain distributions along the center line of BX6100geogrid**

# STABILITY ANALYSIS OF REINFORCED SOIL FOUNDATIONS

Based on the literature review and the results of experimental study the five possible failure modes can be identified for reinforced soil foundations: failure above the top layer of reinforcement (Binquet and Lee, 1975); failure between reinforcement layers (Wayne et al., 1998); failure similar to footings on a two layer soil system (strong soil layer over weak soil layer) (Wayne et al., 1998); bearing failure within the reinforced zone; and partial punching-shear failure in the reinforced zone. The first two failure modes can be avoided by keeping the top layer spacing ($u$) and the vertical spacing between the reinforcement layers ($h$) small enough. The results of experimental studies showed that the top layer spacing ($u$) and the vertical spacing ($h$) need to be less than $0.5B$ to prevent these two failure modes from occurring, where $B$ is the width of footing. This requirement is not difficult to fulfill in engineering practice, and therefore, the discussion here will be focused only on the latter three failure modes. The authors' observations from this experimental study showed that the orientation of geosynthetic reinforcements at the ultimate load is close to the horizontal direction in reinforced, clayey and sandy soil; the "confinement effect" is therefore believed to be the dominant reinforcing mechanism in reinforced clayey and sandy soils. However, for reinforced crushed limestone, due to its relatively larger particle sizes, the reinforcement is believed to move together with the aggregates and therefore the "membrane effect" is considered the major reinforcing mechanism in reinforced crushed limestone. These two effects will lead to an increase in the bearing capacity of reinforced soils, and hence the contribution of reinforcements to the increase in the bearing capacity needs to be included in the design calculation.

The existing analytical solutions available in literature were first examined by comparing the predicted bearing capacities from these methods with the measured values from the small-scale and large-scale model footing tests conducted in this study. The results of comparison showed that none of the existing methods were able to give a good prediction of the measured capacities. Most of these solutions overestimate the results of model tests. Stability analyses of reinforced soil foundations were then performed to develop more rational analytical models for evaluating the ultimate bearing capacity of reinforced soil foundations for different soil types.

### Analytical Solution for Reinforced Silty Clay Soil

Due to the cohesive nature of silty clay soil, the failure mechanism of footing on a two layer system (strong soil layer over weak soil layer) controls the performance of reinforced clayey soils. In this mechanism, a punching shear failure will occur in the reinforced zone, followed

by a general shear failure in the unreinforced zone, as shown in figure 13. This type of failure mode was first suggested by Meyerhof and Hanna (1978) for stronger soil underlying by weaker soil. With some modification, Meyerhof and Hanna's solution can be used to calculate the bearing capacity of reinforced soil foundation (Wayne et al., 1998).

Considering the strip footing case, as shown in figure 13, the forces on the vertical punching failure surfaces *aa'* and *bb'* in the upper soil layer include the total passive earth pressure $P_p$, inclined at an average angle $\delta$, and adhesive force $C_a = c_a d$ acting upwards; where $c_a$ is the unit adhesion of soil along two sides and $d$ is the depth of reinforcement. With the inclusion of reinforcement, an upward shear force $F_T = \sum(T_i tan\delta)$ will be induced by the tension effect of reinforcement on the vertical failure surface; where $T_i$ is the tensile force in the $i^{th}$ layer of reinforcement and $\delta$ is the mobilized friction angle along two sides. The determination of $T_i$ will be discussed in subheading, "Tensile Force in Reinforcement."

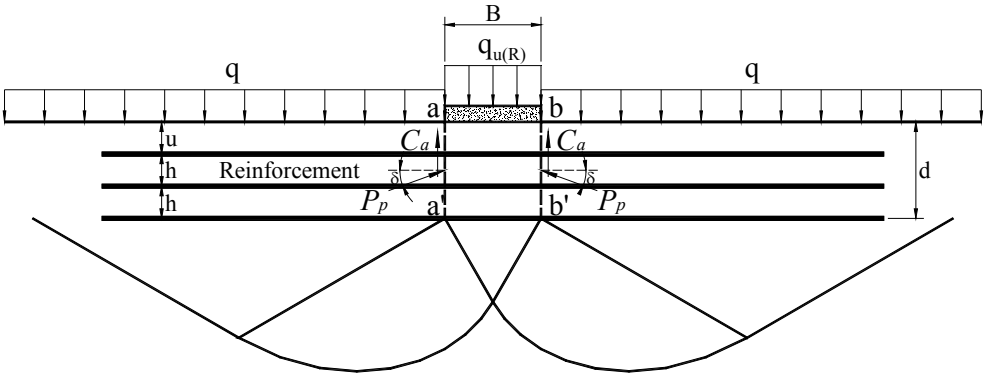


**Figure 13**
**Failure mode of silty clay**

The ultimate bearing capacity of reinforced silty clay soil can be given by modifying Meyerhof and Hanna's solution to incorporate the confinement effect of reinforcement as follows for strip footing on a reinforced silty clay soil:

$$q_{u(R)} = q_{u(b)} + \frac{2c_a d}{B} + \gamma d^2 \left(1 + \frac{2D_f}{d}\right) \frac{K_s \tan\phi}{B} + \frac{2\sum_{i=1}^{N} T_i \tan\delta}{B} - \gamma d \qquad (1)$$

where $q_{u(R)}$ is the ultimate bearing capacity of reinforced soil foundation, $q_{u(b)}$ is the ultimate bearing capacity of the underlying unreinforced soil; $\gamma$ is the unit weight of soil; $B$ is the footing width; $D_f$ is the embedment depth of the footing; $K_s$ is the punching shear coefficient,

which depends on the friction angle of soil in the reinforced zone and the ultimate bearing capacity of soil in both the reinforced zone and the underlying unreinforced zone; $\phi$ is the friction angle of soil in the reinforced zone; and $N$ is the number of reinforcement layers. The punching shear coefficient, $K_s$, can be obtained from figure 14. For uniform soil, i.e., the same soil in both reinforced and underlying unreinforcecd zone, the unit adhesion, $c_a$, equals to the soil cohesion, $c$, and the mobilized friction angle, $\delta$, equals to the friction angle, $\phi$.

Similar to equation (1), the formula for ultimate bearing capacity of square footings on a reinforced silty clay soil can be given as:

$$q_{u(R)} = q_{u(b)} + \frac{4c_a d}{B} + 2\gamma d^2\left(1+\frac{2D_f}{d}\right)\frac{K_s \tan\phi}{B} + \frac{4\sum_{i=1}^{N} T_i \tan\delta}{B} - \gamma d \qquad (2)$$

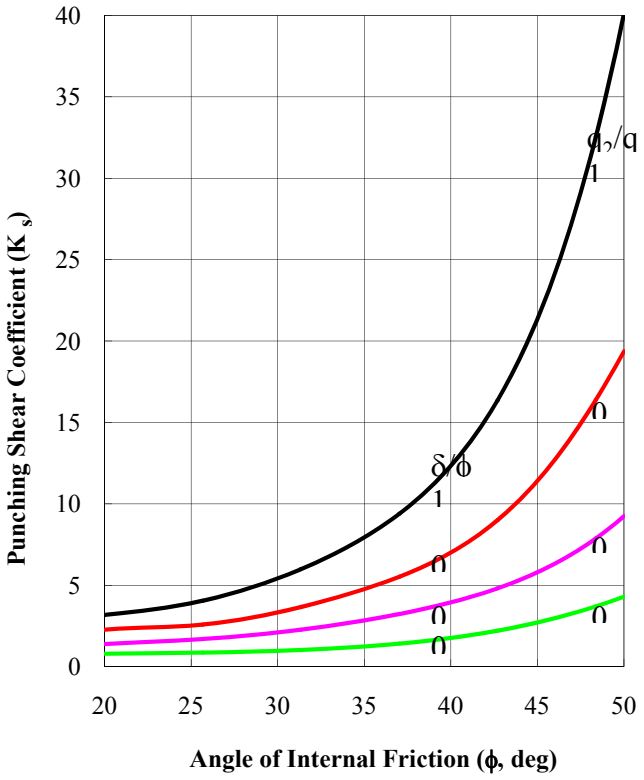


**Figure 14**
**Coefficients of punching shear resistance under vertical load**
**(after Meyerhof and Hanna, 1978)**

**Analytical Solution for Reinforced Sand Soil**

Due to the flowability of sand, the failure of reinforced sand most likely occurs in the reinforced zone, as shown in figure 15.

To include the contribution of reinforcement, the method of superposition was used and an additional term, $\Delta q_T$, was added to include the effect of tensile force $T$. The bearing capacity equation for strip footing on reinforced sand will then be given as follows:

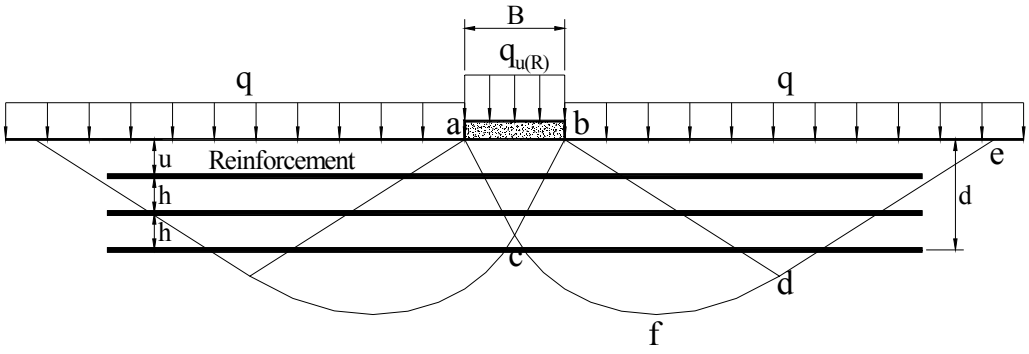


**Figure 15**
**Failure mode of sand**

$$q_{u(R)} = q_{u(UR)} + \Delta q_T = cN_c + qN_q + 0.5\gamma BN_\gamma + \Delta q_T \tag{3}$$

where, $q_{u(UR)}$ is the bearing capacity of unreinforced soil foundation, $\Delta q_T$ is the increased bearing capacity due to the tensile force of the reinforcement, $c$ is the cohesion of soil, $q$ is the surcharge load, and $N_c$, $N_q$, and $N_\gamma$ are the bearing capacity factors, which are dependent on the friction angle of soil $\phi$.

For the case of strip footing on reinforced sand, the increased bearing capacity, $\Delta q_T$, can be given as:

$$\Delta q_T = \sum_{i=1}^{N} \frac{4T_i\left[u + (i-1)h\right]}{B^2} \tag{4}$$

where, $T_i$ is the tensile force in the $i^{\text{th}}$ reinforcement layer, $u$ is the depth of first reinforcement layer, and $h$ is the reinforcement spacing. The ultimate bearing capacity of the strip footing on reinforced sand soil can then be given as follows:

$$q_{u(R)} = cN_c + qN_q + 0.5\gamma BN_\gamma + \sum_{i=1}^{N} \frac{4T_i\left[u + (i-1)h\right]}{B^2} \tag{5}$$

Similarly, the ultimate bearing capacity of the square footing on reinforced sand soil can be given as:

$$q_{u(R)} = 1.3cN_c + qN_q + 0.4\gamma BN_\gamma + \sum_{i=1}^{N} \frac{12T_i\left[u + (i-1)h\right]r_T}{B^2} \tag{6}$$

where:

$$r_T = \begin{cases} \left[1 - 2\dfrac{u + (i-1)h}{B} tan\left(\dfrac{\pi}{4} - \dfrac{\phi}{2}\right)\right] & \text{for} \quad u + (i-1)h < \dfrac{B}{2} tan\left(\dfrac{\pi}{4} + \dfrac{\phi}{2}\right) \\ \dfrac{1}{2} - \dfrac{u + (i-1)h}{2H_f} & \text{for} \quad u + (i-1)h \geq \dfrac{B}{2} tan\left(\dfrac{\pi}{4} + \dfrac{\phi}{2}\right) \end{cases} \tag{7}$$

where, $H_f$ is the depth of failure surface and can be evaluated as:

$$H_f = \frac{B}{2\cos(\pi/4 + \phi/2)} e^{(\pi/4 + \phi/2)\tan\phi} \cos\phi \tag{8}$$

**Analytical Solution for Reinforced Crushed Limestone**

Based on the test results of this study, the failure mechanism in reinforced crushed limestone was identified to be as shown in figure 16, i.e., partial punching shear failure in the reinforced zone followed by a general shear failure below it. As shown in the figure, the forces on the vertical punching failure surfaces *aa'* and *bb'* include the total passive earth pressure $P_p$, inclined at an average angle $\delta$, and adhesive force $C_a = c_a D_P$ acting upwards; where $D_P$ is the depth of the punching shear failure in the reinforced zone. For crushed limestone, due to its relatively large particle size, the geogrid reinforcement is believed to move together with the soil wedge *abb'ca'* as shown in figure 16. An upward force along the failure surfaces will be induced by the tension effect of reinforcement on the failure surfaces.

To estimate the ultimate bearing capacity of reinforced crushed limestone, Meyerhof and Hanna's solution for footings on a two-layer soil system was modified, and an additional term $\Delta q_T$ was added to include the effect of tensile force of reinforcement *T*.

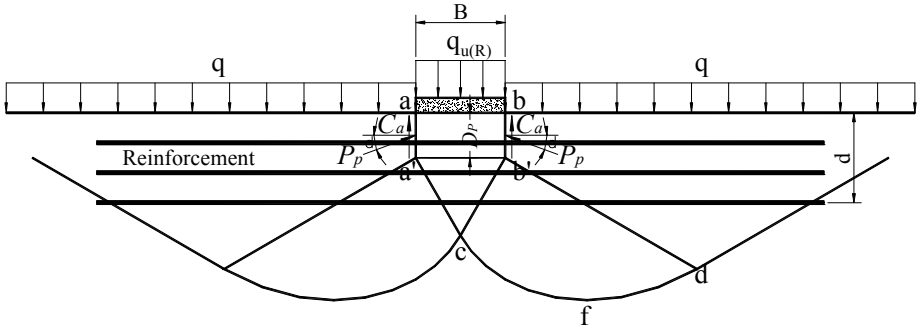


**Figure 16**
**Failure mode of reinforced crushed limestone**

For strip footing, the ultimate bearing capacity of reinforced crushed limestone can be given as follows:

$$q_{u(R)} = q_{u(g)} + \frac{2c_a D_P}{B} + \gamma D_P{}^2\left(1+\frac{2D_f}{D_P}\right)\frac{K_s \tan\phi}{B} - \gamma D_P + \Delta q_T \tag{9}$$

$$\Delta q_T = 2\sum_{i=1}^{N_P}\frac{T_i}{B} + \sum_{i=N_P+1}^{N}\frac{2T_i \sin\left(\frac{\pi}{4}+\frac{\phi}{2}\right)}{B} \tag{10}$$

where, $q_{u(R)}$ is the ultimate bearing capacity of reinforced soil foundation, $q_{u(g)}$ is the ultimate bearing capacity of unreinforced soil located in the general shear failure zone, $D_P$ is the depth of the punching shear failure in the reinforced zone= $d/4$, $d$ is the depth of reinforced zone, $T_i$ is the tensile force in the $i^{th}$ layer of reinforcement, and $N_p$ is the number of reinforcement layers located in the punching shear failure zone.

Similarly, the ultimate bearing capacity of the square footing on a reinforced crushed limestone can be evaluated as:

$$q_{u(R)} = q_{u(g)} + \frac{4c_a D_P}{B} + 2\gamma D_P{}^2\left(1+\frac{2D_f}{D_P}\right)\frac{K_s \tan\phi}{B} - \gamma D_P + \Delta q_T \tag{11}$$

$$\Delta q_T = 4\sum_{i=1}^{N_P}\frac{T_i}{B} + \sum_{i=N_P+1}^{N}\frac{4T_i \sin\left(\frac{\pi}{4}+\frac{\phi}{2}\right)\left\{B-2\left[u+(i-1)h-D_P\right]\tan\left(\frac{\pi}{4}-\frac{\phi}{2}\right)\right\}}{B^2} \tag{12}$$

**Tensile Force in Reinforcement**

To calculate the ultimate bearing capacity of reinforced soil foundation using the proposed analytical solutions, it is critical to find a reasonable procedure to estimate the tensile forces in the reinforcement layers, $T_i$.

**Reinforced Silty Clay**

Based on the strain distribution measured along the reinforcements in reinforced silty clay soil, it is recommended for design purposes to use maximum mobilized tensile strain values, $\varepsilon_{max}$, of 2 percent and 0.5 percent for the points beneath the center of footing for the top and bottom reinforcement layers, respectively. The corresponding strain for reinforcements located between the top and bottom layers can be linearly interpolated. A triangular distribution, as shown in figure 17, is assumed here to describe the approximate strain distribution along the reinforcement. The tensile force, $T$, developed at a certain point in reinforcement can then be evaluated by the following equation:

$$T_i = J\varepsilon_i \tag{13}$$

where, $J$ is the tensile modulus of reinforcement, and $\varepsilon_i$ is the strain at a certain point in the reinforcement $i$.

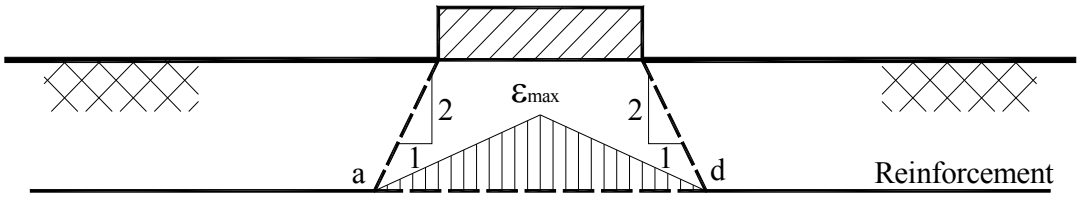


**Figure 17**
**Simplified strain distribution along the reinforcement**

**Reinforced Sand**

The shape of reinforcement (or vertical settlement distribution) in sand soil can be assumed to follow the simplified form shown in figure 18. The reinforcement beneath the footing is assumed to move downward uniformly (lines *bc*). The reinforcement located outside of a certain boundary (lines *a-a'* and *d-d'*) is considered to have negligible strain.

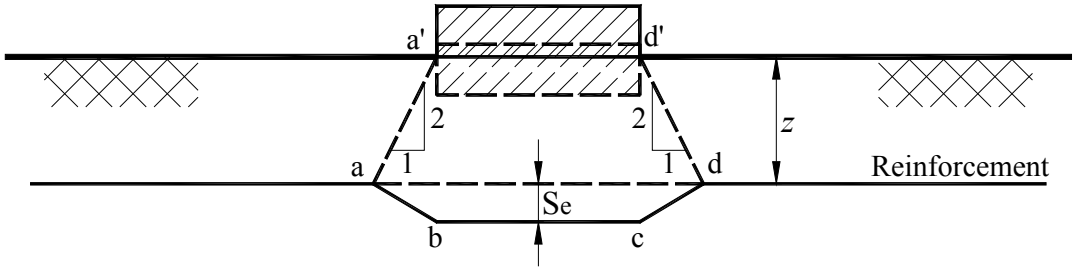


**Figure 18**
**Simplified distribution of vertical settlement in sand**

To calculate the elastic settlement $S_e$ at any depth in sand, we can integrate the strain in sand below this depth with respect to depth, and the following formula suggested by Schmertmann et al. (1978) can be applied:

$$S_e = C_1 C_2 C_3 \left(q - \gamma D_f\right) \sum \frac{I_\varepsilon \Delta z}{E_s} \tag{14}$$

$$C_1 = 1 - 0.5 \frac{\gamma D_f}{q - \gamma D_f} \tag{15}$$

$$C_2 = 1 + 0.2 \log\left(\frac{t}{0.1}\right) \tag{16}$$

$$C_3 = 1.03 - 0.03 L/B \geq 0.73 \tag{17}$$

where, $C_1$ is a correction factor for the depth of embedment; $C_2$ is a correction factor for secondary creep in sand; $C_3$ is a correction factor for the footing shape; $q$ is the surcharge load; $D_f$ is the embedment depth of the footing; $I_\varepsilon$ is the strain influence factor; $\Delta z$ is the thickness of subdivided soil layer; $E_s$ is the elastic modulus of sand; $t$ is the time since application of load (yr) ($t \geq 0.1$yr)); and $L$ is the length of footing; $B$ is the width of the footing. Schmertmann et al. (1978) suggested a practical distribution of strain influence factor ($I_{\varepsilon z}$) along the depth below the footings as shown in figure 19. The peak value of the strain influence factor $I_{\varepsilon p}$ is evaluated by the following equation:

$$I_{\varepsilon p} = 0.5 + 0.1\sqrt{\frac{q - \gamma D_f}{\sigma_{vp}'}} \tag{18}$$

$$\sigma_{vp}' = \gamma\left(D_f + B/2\right) \text{ (square footing)} \tag{19}$$

$$\sigma_{vp}' = \gamma\left(D_f + B\right) \text{ (strip footing)} \tag{20}$$

where, $q$ is the bearing pressure of footing.

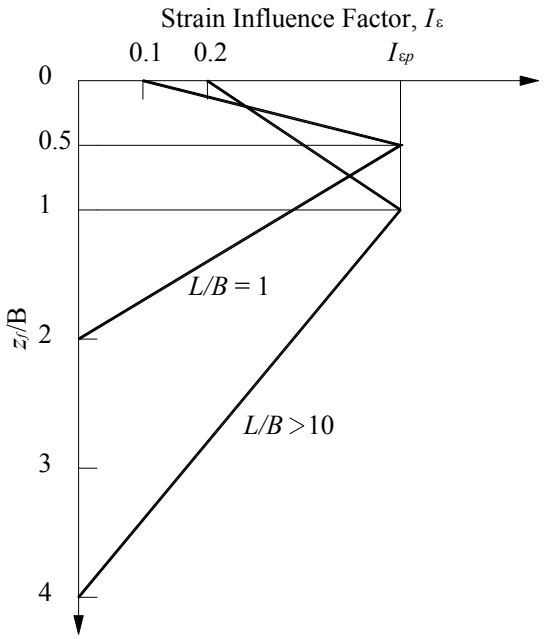


**Figure 19**
**Strain influence factor distribution diagrams (after Schmertmann et al., 1978)**

Based on the above assumptions and analysis, the average strain ($\varepsilon_{avg}$) for a reinforcement layer at depth z below footing for a given footing settlement can be calculated as:

$$\varepsilon_{avg} = \frac{L_{ab} + L_{bc} + L_{cd} - L_{ad}}{L_{ad}} = \frac{\Delta L}{L_{ad}} \tag{21}$$

$$\Delta L = 2\sqrt{S_e^2 + (z/2)^2} - z \tag{22}$$

A triangle distribution, as shown in figure 17 is again assumed here again to describe the approximate strain distribution along the reinforcement. The tensile force $T_i$, developed in a reinforcement layer *i*, can be evaluated using equation (13).

**Reinforced Crushed Limestone**

The shape of reinforcement (or vertical settlement distribution) in crushed limestone can be assumed to follow the simplified form shown in figure 20. The reinforcement in the soil wedge beneath the footing is assumed to move down uniformly (lines *cd*). The reinforcement outside of the wedge is taken as horizontal. The strain of the reinforcement beyond a certain boundary (lines *a-a'* and *f-f'*) is considered to be insignificant.

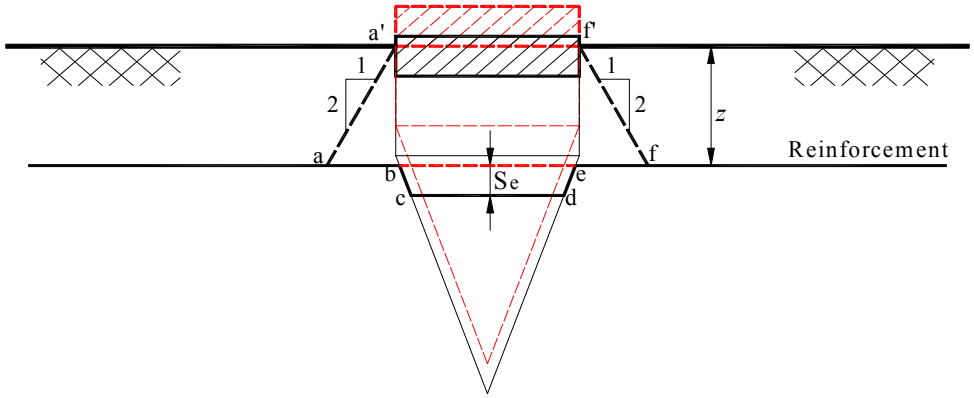


**Figure 20**
**Simplified shape of reinforcement in crushed limestone**

The magnitude of elastic settlement ($S_e$) in crushed limestone at a certain depth z beneath the footing can be evaluated using Schmertmann's method, similar to sand soil. To calculate $S_e$ at any depth, one can integrate the strain below this depth and then apply equation (14).

Based on the above assumptions and analyses, the average strain ($\varepsilon_{avg}$) in reinforcement at depth z below the footing for a certain footing settlement can now be calculated as:

$$\varepsilon_{avg} = \frac{L_{ab} + L_{bc} + L_{cd} + L_{de} + L_{ef} - L_{af}}{L_{af}} = \frac{\Delta L}{L_{af}} \tag{23}$$

$$\Delta L = 2S_e - 2A + 2A \Big/ \sin\left(\frac{\pi}{4} + \frac{\phi}{2}\right) - 2A \cdot tg\left(\frac{\pi}{4} - \frac{\phi}{2}\right) \tag{24}$$

where:

$$A = \begin{cases} 0 & \text{for } z \le D_P \\ S_e & \text{for } z > D_P \text{ and } S_e \le z - D_P \\ z - D_P & \text{for } z > D_P \text{ and } S_e > z - D_P \end{cases} \tag{25}$$

where, $S_e$ is the settlement at a depth $z$ beneath the center of footing; $z$ is the depth of reinforcement = $u$ + ($i$-1) $h$.

A triangle distribution, as shown in figure 17 is again assumed to describe the approximate strain distribution along the reinforcement. The tensile force, $T_i$, developed in a reinforcement layer $i$, can be evaluated using equation (13).

## Verification of Analytical Model

The large number of laboratory model tests on reinforced sand and silty clay soils conducted in this research program provides the experimental data needed to verify/compare the analytical solutions described herein. The bearing capacity ratio (BCR) is used here to compare between the results of laboratory model tests and the predicted values from analytical solutions. The predicted ultimate bearing capacity ratios of the reinforced soils were calculated based on aforementioned failure modes. The comparison between the results of laboratory model tests and the predicted values from proposed analytical solution using equation (2) is presented in figure 21 for BasXgrid 11 geogrid reinforced silty clay soil. Figures 22 and 23 presents the comparisons for BasXgrid 11 geogrid reinforced sand using equation (6) and BX1200 geogrid reinforced crushed limestone using equation (11), respectively. More comparisons can be found in the final report. As indicated in these figures, the proposed analytical solution provides a good prediction of BCR for the model footing tests.

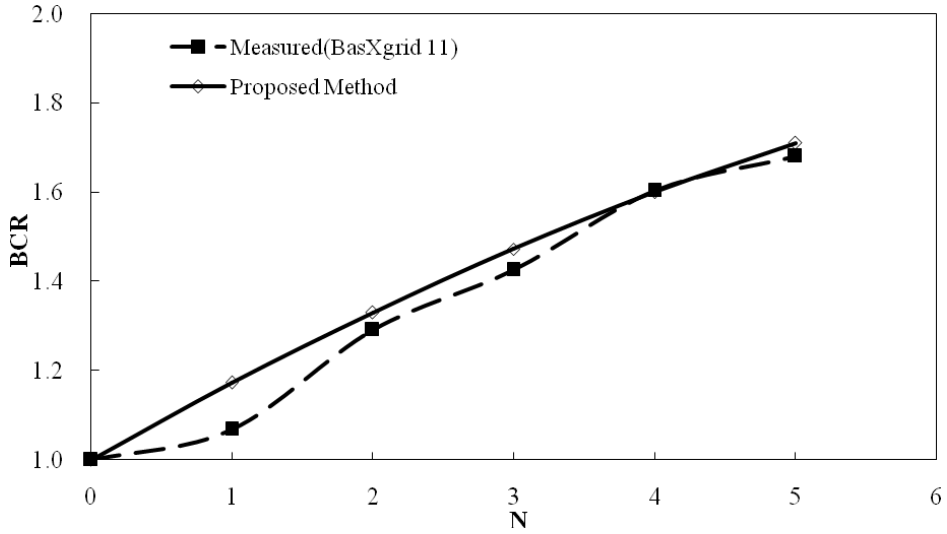


**Figure 21**
**BCR vs. number of layers (N) for reinforced silty clay with BasXgrid11 geogrid**

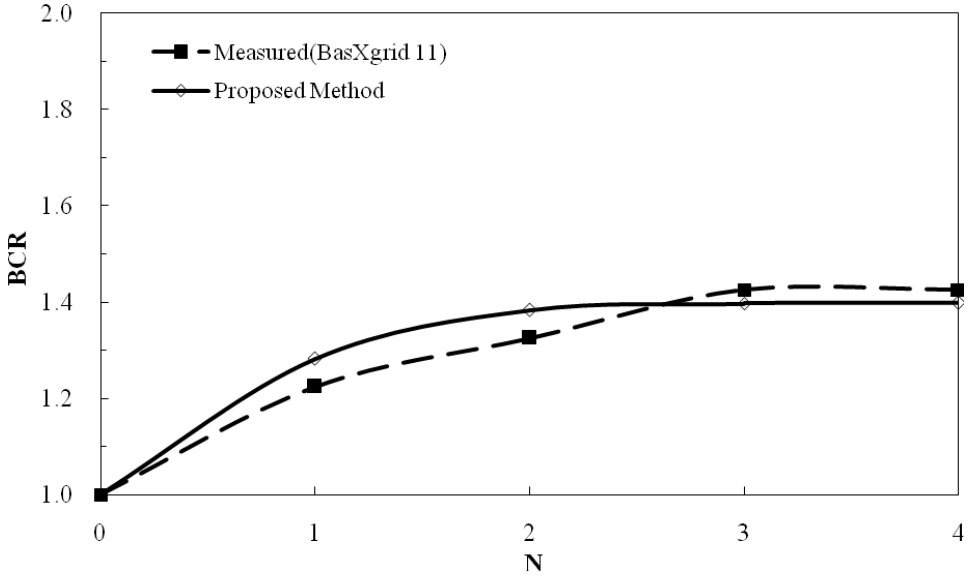


**Figure 22**
**BCR vs. number of layers (N) for reinforced sand with BasXgrid11 geogrid ($D_f/B = 0.0$)**

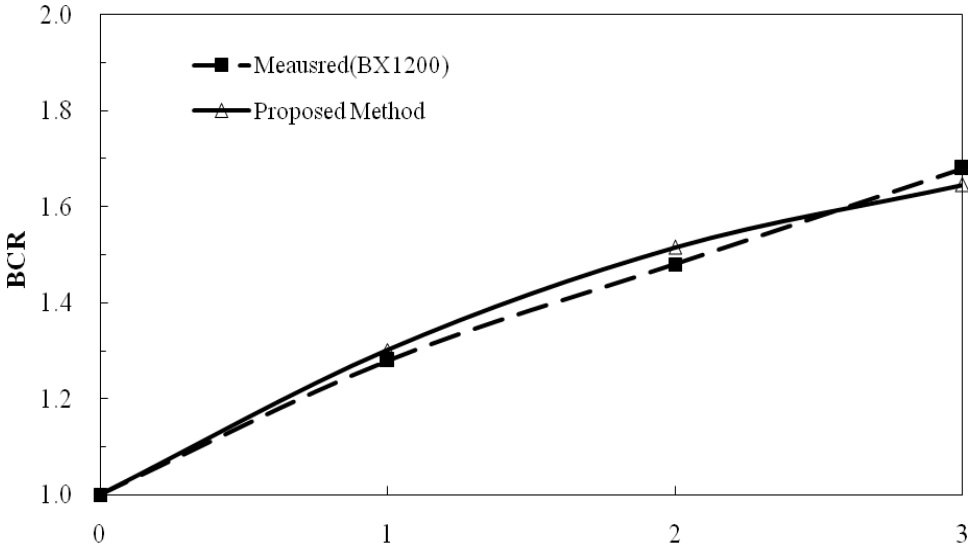


**Figure 23**
**BCR vs. number of layers (N) for reinforced crushed limestone with BX1200 geogrid**

# CALCULATION EXAMPLE

## Example 1: Reinforced Sand

To illustrate the analytical model, example calculations are presented for a case adopted from model tests presented by Adams and Collin (1997).

The following data are given:

$B$ = 2 ft., $D_f$ = 0.0 ft., $\gamma$ = 92.3 pcf, $N$ = 2, $u/B$ = 0.25, $h/B$ = 0.25, $q_u$ = 39.2 psi (unreinforced, at $s/B$ = 10%), $J$ = 30830 lb/ft (average value in machine and cross-machine direction).

The following data are back-calculated:

$\phi = 37.9^{o}$, $E_s$ = 511.3 psi

**Step 1**

Calculating the settlement at the first and second layers of reinforcement:

$C_1 = 1$, $C_2 = 1$, $C_3 = 1$

First Layer (at a depth of $z_1 = u$):

| $\Delta z$ (in.) | $E_s$ (psi) | z (in.) | $I_\varepsilon$ | $I_\varepsilon \Delta z/E_s$ |
|---|---|---|---|---|
| 6 | 511.3 | 9 | 0.986 | 0.043 |
| 6 | 511.3 | 15 | 1.175 | 0.051 |
| 6 | 511.3 | 21 | 0.961 | 0.042 |
| 6 | 511.3 | 27 | 0.747 | 0.032 |
| 6 | 511.3 | 33 | 0.534 | 0.023 |
| 6 | 511.3 | 39 | 0.320 | 0.014 |
| 6 | 511.3 | 45 | 0.107 | 0.005 |
| | | | $\Sigma$ | 0.209 |

$$S_{e1} = C_1 C_2 C_3 (q - \gamma D_f) \sum \frac{I_\varepsilon \Delta z}{E_s}$$

$= (1)(1)(1)(39.2 - 0)(0.209)$

$= 2.221$ *in.*

Second Layer (at a depth of $z_2 = u+h$):

| Δz (in.) | $E_s$ (psi) | z (in.l) | $I_\varepsilon$ | $I_\varepsilon \Delta z/E_s$ |
|---|---|---|---|---|
| 6 | 511.3 | 15 | 1.175 | 0.051 |
| 6 | 511.3 | 21 | 0.961 | 0.042 |
| 6 | 511.3 | 27 | 0.747 | 0.032 |
| 6 | 511.3 | 33 | 0.534 | 0.023 |
| 6 | 511.3 | 39 | 0.320 | 0.014 |
| 6 | 511.3 | 45 | 0.107 | 0.005 |
| | | | Σ | 0.166 |

$$S_{e2} = C_1 C_2 C_3 \left(q - \gamma D_f\right) \sum \frac{I_\varepsilon \Delta z}{E_s}$$

$$= (1)(1)(1)(39.2 - 0)(0.166)$$

$$= 1.768 \; in.$$

**Step 2**

Calculating the tensile forces in the first and second layers of reinforcement:

First Layer:

$$L_{ab} = L_{cd} = \sqrt{s_{e1}^2 + \left(z_1/2\right)^2} = \sqrt{2.221^2 + \left(6/2\right)^2} = 3.734 \; in.$$

$$L_{bc} = B = 24 \; in.$$

$$L_{ad} = B + z_B = 24 + 6 = 30 \; in.$$

Average strain:

$$\varepsilon_{avg} = \frac{L_{ab} + L_{bc} + L_{cd} - L_{ad}}{L_{ad}} = \frac{3.734 + 24 + 3.734 - 30}{30} = 4.88\%$$

$$\varepsilon_{\max} = 2\varepsilon_{avg} = 2 \times 4.88\% = 9.76\%$$

Strain at the triangle soil wedge faces *ac* and *bc* as shown in figure 15:

$$\varepsilon = \frac{\dfrac{u}{\tan\left(\pi/4 + \phi/2\right)} + \dfrac{u}{2}}{\dfrac{B+u}{2}} \varepsilon_{\max} = 3.86\%$$

$$T_1 = J\varepsilon = 30830 \cdot 3.86\% = 1192 \; lb/ft$$

Second Layer:

$$L_{ab} = L_{cd} = \sqrt{s_{e1}^2 + (z_2/2)^2} = \sqrt{1.768^2 + (12/2)^2} = 6.259\ in.$$

$$L_{bc} = B = 24\ in.$$

$$L_{ad} = B + z_B = 24 + 12 = 36\ in.$$

$$\varepsilon_{avg} = \frac{L_{ab} + L_{bc} + L_{cd} - L_{ad}}{L_{ad}} = \frac{6.259 + 24 + 6.259 - 36}{36} = 1.415\%$$

$$\varepsilon_{\max} = 2\varepsilon_{avg} = 2 \times 1.415\% = 2.83\%$$

$$\varepsilon = \frac{\dfrac{u+h}{\tan(\pi/4 + \phi/2)} + \dfrac{u+h}{2}}{\dfrac{B+u+h}{2}} \varepsilon_{\max} = 1.87\%$$

$$T_2 = J\varepsilon = 30830 \cdot 1.87\% = 575.583\ lb/ft$$

**Step 3**

Calculating the increased bearing capacity $\Delta q_T$:

$$\Delta q_T = \sum_{i=1}^{N} \frac{12T_i\left[u + (i-1)h\right]\left[1 - 2\dfrac{u + (i-1)h}{B}\tan\left(\dfrac{\pi}{4} - \dfrac{\phi}{2}\right)\right]}{B^2} = 15.5\ psi$$

**Step 4**

Calculating the ultimate bearing capacity of reinforced sand:

$$q_{u(R)} = q_u + q_T = 1.3cN_c + qN_q + 0.4\gamma BN_\gamma + \Delta q_T = 39.2 + 15.5 = 54.7\ psi$$

**Example 2: Reinforced Silty Clay**

To illustrate the analytical model, example calculations are presented for five layers of BX6200 geogrid placed at 6 in. spacing.

The following data are given:

$B$ = 18 in., $D_f$ = 0.0 in., $\gamma$ = 110 pcf, $N$ = 5, $u/B$ = 1/3, $h/B$ = 1/3, $q_u$ = 130 psi (unreinforced, at $s/B$=10%), $J$ = 22130 lb. /ft. (average value in machine and cross-machine direction).

The following data are back-calculated:

$c$=3.63 psi, $\phi = 28^o$

**Step 1**

The tension developed in the reinforcement at different levels (based on measuring strain):

$T_1$ = 181.6 lb./ft., $T_2$ = 153.5 lb./ft., $T_3$ = 125.4 lb./ft., $T_4$ = 97.3 lb./ft., $T_5$ = 69.2 lb./ft.

**Step 2**

Calculating the ultimate bearing capacity of the underlying unreinforced silty clay:

$N_q = 14.72, \quad N_c = 25.8, \quad N_\gamma = 16.72, \quad d = 30\ in.$

$q_b = 1.3cN_c + \gamma\left(d + D_f\right)N_q + 0.4\gamma BN_\gamma = 157.5\ psi$

**Step 3**

Calculating the ultimate bearing capacity of the reinforced silty clay:

$K_s$ = 4.796, $c_a$ = 3.63 psi, $\delta = 28^o$

$$q_{u(R)} = q_b + \frac{4c_a d}{B} + 2\gamma_t d^2\left(1 + \frac{2D_f}{d}\right)\frac{K_s \tan\phi}{B} - \gamma_t d + \frac{4\sum_{i=1}^{N} T_i \tan\delta}{B} = 202 \text{ psi}$$

# CONCLUSIONS

Based on the results of the present study, the following conclusions can be drawn:

(1) The inclusion of reinforcement generally increased the ultimate bearing capacity of soil and reduced the footing settlement.

(2) The optimum depth of the first reinforcement layer was estimated to be at 0.33B below footing for all soils tested in this study.

(3) The bearing capacity of reinforced soil increases with increasing number of reinforcement layers. However, the significance of an additional reinforcement layer decreases with the increase in number of layers. The reinforcing effect becomes negligible below the influence depth. The influence depth of reinforced sand was obtained at approximately 1.25B regardless of the type of reinforcement and footing embedment depth; while the influence depth of geogrid and geotextile reinforced silty clay was obtained as about 1.5B and 1.25B, respectively.

(4) The BCR values decrease with increasing the vertical spacing of reinforcement layers. For the tested soils and geogrid reinforcements, one can realize that the smaller the spacing, the higher the BCR. In practice, the cost would govern the spacing and require 6 in. $\leq$ h $\leq$ 18 in. For design purposes, engineers need to balance between reducing spacing and increasing geogrid tensile modulus. However, the authors believe that an $h/B$ = 0.33 can be a reasonable value for use in the design of reinforced soil.

(5) Geogrid beyond the effective length (4.0 ~ 6.0B) results in insignificant mobilized tensile strength and thus provides negligible reinforcement effect.

(6) In general, the performance of reinforced soil improves with increasing the reinforcement tensile modulus. For a project controlled by settlement criteria, geogrid reinforcement is generally considered to perform better for soil foundation than geotextile.

(7) The inclusion of reinforcement will redistribute the applied load to a wider area, thus minimizing stress concentration underneath footing. The redistribution of stresses below the reinforced zone will result in reducing the total consolidation settlement of the underlying weak clayey soil which is directly related to the induced stress.

(8) The strain developed along the reinforcement is directly related to the settlement, and therefore higher tension would be developed for geogrids with higher modulus under the same footing settlement.

(9) Failure mechanisms were proposed for RSFs of different soil types based on the literature

review and the results of model tests. Stability analyses were then conducted on the proposed failure mechanisms to evaluate the contribution of reinforcement in terms of the increase in soils' bearing capacity, and new models were developed for RSFs of three soil types. A reasonable estimation of the tensile force along the reinforcement was also proposed.

(10) The proposed methods provide good predictions of laboratory model test results of this study. The predicted bearing capacities of reinforced soil foundation by using the methods of this study are also in good agreement with the field test results of previous research for reinforced sand and this study for reinforced silty clay.

# RECOMMENDATIONS

Based on extensive laboratory and field model footing tests, the following step-by-step procedure is recommended for the design of reinforced soil foundations.

(1) Assume the footing width, $B$.

(2) Determine the bearing pressure along the bottom of a shallow foundation, $q$.

(3) Select the geogrid with specific tensile modulus ($J$), which can be obtained from geogrid manufactures, and the proper reinforcement layout. Based on the experimental test results of this study, typical design parameters for reinforcement layout are recommended in table 5.

(4) Determine the possible failure mode of reinforced soil foundation based on the soil type in the field.

(5) Determine the tensile forces, $T_i$, developed in the reinforcement layers using the methods proposed in this study (refer to section "tensile force in reinforcement").

(6) Calculate the ultimate bearing capacity of unreinforced soil foundation, $q_{u(UR)}$.

(7) Calculate the ultimate bearing capacity of reinforced soil foundation, $q_{u(R)}$ by using equation (1) or (2) for clay, (5) or (6) for sand, and (9) or (11) for limestone.

(8) Calculate the allowable bearing capacity of reinforced soil foundation, $q_{a(R)}$ as

$$q_{a(R)} = \frac{q_{u(R)}}{F_S} \tag{26}$$

where, $F_s$ is the factor of safety.

(9) If the allowable bearing capacity of reinforced soil foundation, $q_{a(R)}$, is lower than the bearing pressure, $q$, repeat steps (1) through (8) for different reinforcement layout.

**Table 5**
**Recommended design parameters for reinforcement layout**

| Parameter | Typical value | Recommended |
|---|---|---|
| $u/B$ | 0.2 ~ 0.5 | 1/3 |
| $h/B$ | 0.2 ~ 0.5 | 1/3 |
| $d/B$ | 1.3 ~ 1.7 | 1.5 |
| $l/B$ | 4 ~ 6 | 5 |

# REFERENCES


1. Adams, M.T., and Collin, J.G., "Large Model Spread Footing Load Tests on Geosynthetic Reinforced Soil Foundations." *Journal of Geotechnical and Geoenvironmental Engineering*, ASCE, Vol. 123, No.1, 1997, pp. 66-72.
2. American Society for Testing and Materials, ASTM D 1196-93, *Standard Test Method for Nonrepetitive Static Plate Load Tests of Soils and Flexible Pavement Components for Use in Evaluation and Design of Airport and Highway Pavements*, Philadelphia, PA. Reapproved 1997, pp.112-113.
3. Binquet, J., and Lee, K.L., "Bearing Capacity Analysis of Reinforced Earth Slabs." *Journal of Geotechnical Engineering Divisio*n, ASCE, Vol. 101, No.GT12, 1975, pp. 1257-1276.
4. Huang, C.C., and Tatsuoka, F., "Bearing Capacity Reinforced Horizontal Sandy Ground." *Geotextiles and Geomembranes*, Vol. 9, 1990, pp. 51-82.
5. Huang, C.C., and Menq, F.Y., "Deep-footing and Wide-slab Effects in Reinforced Sandy Ground." *Journal of Geotechnical and Geoenviromental Engineering*, ASCE, Vol. 123, No.1, 1997, pp. 30-36.
6. Kumar, A., and Saran, S., "Bearing Capacity of Rectangular Footing on Reinforced Soil." *Geotechnical and Geological Engineering*, Vol.21, 2003, pp. 201-224
7. Meyerhof, G.G., and Hanna, A.M., "Ultimate Bearing Capacity of Foundations on Layered Soils Under Inclined Load." *Canadian Geotechnical Journal*, Vol. 15, No.4, 1978, pp. 565-572.
8. Schmertmann, J.H.; Hartman, J.P.; and Brown, P.R., "Improved Strain Influence Factor Diagrams." *Journal of the Geotechnical Engineering Division*, ASCE, Vol. 104, No.GT8, 1978, pp. 1131-1135.
9. Wayne, M.H.; Han, J.; and Akins, K., "The Design of Geosynthetic Reinforced Foundations." *Proceedings of ASCE's 1998 Annual Convention & Exposition*, ASCE Geotechnical Special Publication, 76, 1998, pp. 1-18.
10. Westergaard, H.M., "A Problem of Elasticity Suggested by a Problem in Soil Mechanics: Soft Material Reinforced by Numerous Strong Horizontal Sheets." Contributions to the *Mechanics of Solids*, Dedicated to Stephen Timoshenko, Macmillan, New York, 1938, pp 268 – 277.